ACS OMEGA

Open Access

http://pubs.acs.org/journal/acsodf

Article

Quantitative Analysis of the Influence of Trehalose on Amyloid-β Binding to Membranes by Localized Surface Plasmon Resonance Spectroscopy

Yue Xu, Danielle M. McRae, and Zoya Leonenko*

Cite This: *ACS Omega* 2025, 10, 12872−12879

Read Online

ACCESS | Metrics & More | Article Recommendations | Supporting Information

ABSTRACT: The damaging effect of amyloid-β (Aβ) on cellular membranes is an essential factor that contributes to Aβ's neurotoxicity in Alzheimer's disease. In this work, we explore the role of trehalose sugar in protecting model lipid membranes composed of DPPC-POPC-Cholesterol against Aβ toxicity. We used localized surface plasmon resonance (LSPR) spectroscopy and conducted a quantitative analysis to study the influence of trehalose on Aβ-membrane interactions. The LSPR data indicate that trehalose can effectively reduce the level of binding of Aβ to the lipid membrane, indicating its protective role against amyloid toxicity. Additionally, atomic force microscopy (AFM) was used to visualize the lipid membranes supported on the LSPR sensors and to elucidate the effect of trehalose on membrane morphology. The ability of trehalose to alter the physical properties of model membranes is discussed in relation to its protective role against Aβ during dehydration.

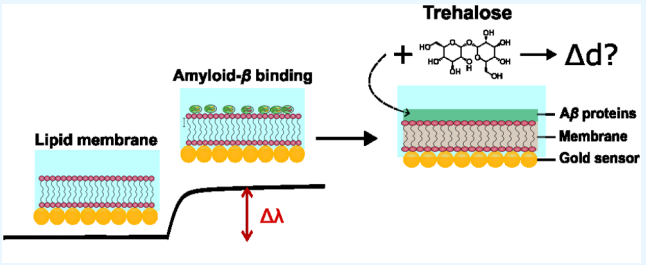

INTRODUCTION

Trehalose, a natural disaccharide that can be found in plants and microbes,[1] is being investigated for the treatment of neurodegenerative diseases involving misfolded proteins in pathogenesis, such as amyotrophic lateral sclerosis (ALS), Huntington's disease, and Alzheimer's disease (AD), among others.[2,3] Animal studies have shown that trehalose exerts its neuroprotective effects through various biological routes during metabolism; this includes modifying and regulating disordered proteins, enhancing antioxidation and anti-inflammation, and modulating gut microbiota,[2] but the mechanisms of trehalose-modulated neuroprotection at the molecular level have not been fully understood.

AD is a progressive neurodegenerative disease that leads to a severe impairment of memory and cognitive function. AD is characterized by the formation of Aβ aggregates on the surfaces of neuronal cells, leading to amyloid plaque formation in individuals with AD.[4−6] The neuronal cell membrane is of critical importance in neural physiology[7] and is recognized as a target for amyloid attack. The role of the lipid membrane on Aβ binding and toxicity has been actively studied.[8−17]

As many drugs targeting toxic Aβ aggregation have failed in clinical trials,[18,19] the role of the cellular membrane itself has been gaining increased interest in this regard[12−14,17,20] and promising ways to protect cellular membranes have been actively investigated.[15,16,21−23] While trehalose has been shown to affect the misfolding and aggregation of Aβ,[24,25] its effects are more promising with less toxic Aβ1−40 than Aβ1−42.[25−27] Moreover, its role in membrane protection against amyloid toxicity has not been studied until recently.[28]

It has been demonstrated that Aβ can bind to lipid membranes[11−14,29] and cause neuronal membrane impairment,[11,12] leading to homeostasis imbalance and cell death.[30−32] Several mechanisms have been proposed to understand these damaging effects of Aβ on lipid membranes due to its binding to the membrane surface,[12,14,17] including the formation of various defects,[12,17] detergent-like destabilizing of lipid membranes,[33] and ion channel formation.[34] Therefore, finding ways to protect the membrane and to prevent Aβ's binding and damaging the lipid membranes is an important direction in Alzheimer's research. Since trehalose has the unique ability to modify the membrane properties,[35−41] studies exploring the role of trehalose in protecting the lipid membrane against the most toxic Aβ1−42[30,32,42] are highly desirable.

Trehalose is a well-established cryopreservative agent for biomolecules and can stabilize cell membranes under extreme conditions.[1] It can maintain membrane stability by eliminating deleterious phase transitions, thereby maintaining membrane fluidity during dehydration.[1] A potential reason is that

Received: July 31, 2024
Revised: March 17, 2025
Accepted: March 20, 2025
Published: March 25, 2025

trehalose can form hydrogen bonds with water and hydrophilic headgroups of lipids at the water/membrane interface.[35−37] Different hypotheses have been proposed to explain the interaction of trehalose with lipid membranes, such as the water replacement hypothesis,[35,43] water entrapment hypothesis,[38−40] and hydration force hypothesis.[44] Even though the trehalose protection mechanisms are still under debate, evidence has shown that some of these hypotheses could be complementary, conjointly explaining trehalose-mediated membrane protection.[41,45] A simulation study by Maiti and Daschakraborty found that trehalose can simultaneously replace water and form a viscous layer on *Escherichia coli* bacterial membranes,[41] supporting both the water replacement hypothesis and the vitrification hypothesis. Trehalose can compensate for water loss and reduce the dehydration level of the membranes.[41] In addition, the viscous layer formed by trehalose can slow down the motion of lipid molecules, thereby maintaining membrane fluidity.[41]

In relation to amyloid, the role of trehalose in amyloid-membrane interaction has been investigated with single-component lipids and shorter and less toxic amyloid fragments, 1−40 and 29−40.[20,46] Simulation studies by Reddy et al. demonstrated that trehalose increases the insertion of Aβ29−40 in 1,2-dipalmitoyl-*sn*-glycero-3-phosphocholine (DPPC) membranes,[20] due to trehalose promoting the conformational transition of Aβ29−40 monomers from a random coil to an α-helix structure, which facilitates its insertion into lipid membranes.[20] However, another simulation study by Izmitli et al. elucidated that the insertion of Aβ1−40 in 1,2-dipalmitoyl-*sn*-glycero-3-phospho-(1′-rac-glycerol) (DPPG) membranes was decreased by the presence of trehalose in an aqueous environment.[46] Trehalose reduces the insertion depth of Aβ1−40 peptides but speeds up the peptide insertion by mitigating the conformational change upon insertion into membranes.[46] These studies focused on Aβ1−40 fragments rather than the most toxic Aβ1−42.

Given the protective role of trehalose in biomembranes, we proposed that trehalose may protect neuronal membranes against the deleterious effects and disruption induced by the most toxic amyloid, Aβ 1−42. Using the electrophysiology technique, we recently showed that the membrane disruption induced by Aβ1−42 is attenuated by the presence of trehalose in a dose-dependent manner.[28] Based on the protection mechanism of trehalose on membrane stability and integrity, we hypothesized that the binding of trehalose at the hydrophilic region of lipid membranes may establish a barrier to reduce or prevent the binding of Aβ 1−42 to the lipid membrane, thereby attenuating amyloid-induced membrane disruption. Our recent study using nanopore electrophysiology demonstrates that trehalose reduces the damaging effects of Aβ 1−42 on model lipid membranes (measured as membrane leakage due to pore formation);[28] however, the underlying molecular mechanism is still unclear. In order to understand the molecular interplay between trehalose, Aβ 1−42 peptides, and lipid membranes, we used localized surface plasmon resonance (LSPR) spectroscopy and atomic force microscopy (AFM) to study the nonspecific binding of Aβ 1−42 to model lipid membranes in the presence of trehalose in this work. We chose a simple DPPC-POPC-Cholesterol lipid model to mimic neuronal membranes to elucidate the influence of trehalose on nonspecific binding between Aβ and membranes.

MATERIALS AND METHODS

Reagents. 1-palmitoyl-2-oleoyl-glycero-3-phosphocholine (POPC), 1,2-dipalmitoyl-*sn*-glycero-3-phosphocholine (DPPC), cholesterol, trehalose, NaCl, 1,1,1,3,3,3-Hexafluoro-2-propanol (HFIP), and 4-(2-hydroxyethyl)-1-piperazineethanesulfonic acid (HEPES) were obtained from Sigma-Aldrich (ON, Canada). The unfunctionalized gold sensors (SEN-AU-100−10) were purchased from Nicoya Lifesciences (ON, Canada).

Vesicle Preparation. Lipids were suspended in chloroform and combined to reach the target weight ratio of 4:4:2 DPPC/POPC/Cholesterol. Then, the lipid chloroform solution was dried under N_2 flow until all the solvent was evaporated, leaving semitransparent lipid residues at the bottom of the vial. The dried lipids were resuspended in the same aqueous buffer as the corresponding working buffer in LSPR experiments. In order to create vesicle solutions, the aqueous lipid solution underwent sonication for 15 min followed by 15 min of stirring at ambient temperature. This cycle of sonication and stirring was repeated until the solution became transparent, indicating the formation of lipid vesicles. The final vesicle concentration of DPPC/POPC/Cholesterol mixture was 0.5 mg/mL. In addition to DPPC/POPC/Cholesterol vesicles, 0.5 and 1 mg/mL POPC vesicles were also produced in the same way to evaluate the decay length of LSPR sensors.

Aβ Solution Preparation. Aβ1−42 powder was resuspended in HFIP and distributed into aliquots. The centrifuge tubes containing the amyloid solution were placed in a desiccator in the fume hood for 24 h to remove as much HFIP as possible. After 24 h, HFIP was evaporated and amyloid powder was left in the tubes. The distributed amyloid powder was stored in a freezer at −20 °C. Before the LSPR experiments were started, the amyloid powder was resuspended in the working buffer at 50 μM and sonicated for 10 min for monomerization.

LSPR Experiments. The OpenSPR 3.0 instrument from Nicoya Lifesciences (ON, Canada) was used for the detection of lipid and protein binding with and without the presence of trehalose. The real-time recording and data collection were performed with Nicoya Lifesciences software (version 3.11).

Theoretical Background of LSPR. Localized surface plasmon resonance is produced by light incident on a metal nanoparticle, exciting the oscillation of electrons on the metal nanoparticle and generating a locally enhanced electromagnetic field. This results in a strong optical absorption at wavelength λ_m, which is influenced by the dielectric environment in the vicinity of the nanoparticle surface.[47] Any changes in the dielectric environment, such as those involving the change in local refractive index n or adsorbate thickness d due to adsorption of a biomolecule layer, can cause the wavelength shift $\Delta\lambda$

$$\Delta\lambda = m\Delta n\left[1 - \exp\left(-\frac{d}{\delta}\right)\right] \quad (1)$$

Here, m is the bulk sensitivity of the sensor, and δ is the decay length of the intensity of the electromagnetic (EM) field,[48,49] also known as the probe length of the sensor.[50,51] It is worth denoting that δ can be substituted by $\frac{l_d}{2}$ in eq 1, as reported.[47,50] Distinct from δ, l_d is the characteristic decay length of the EM field, which is twice the value of δ. The binding or adsorption of biomolecules to the LSPR sensors

https://doi.org/10.1021/acsomega.4c07038
ACS Omega 2025, 10, 12872−12879

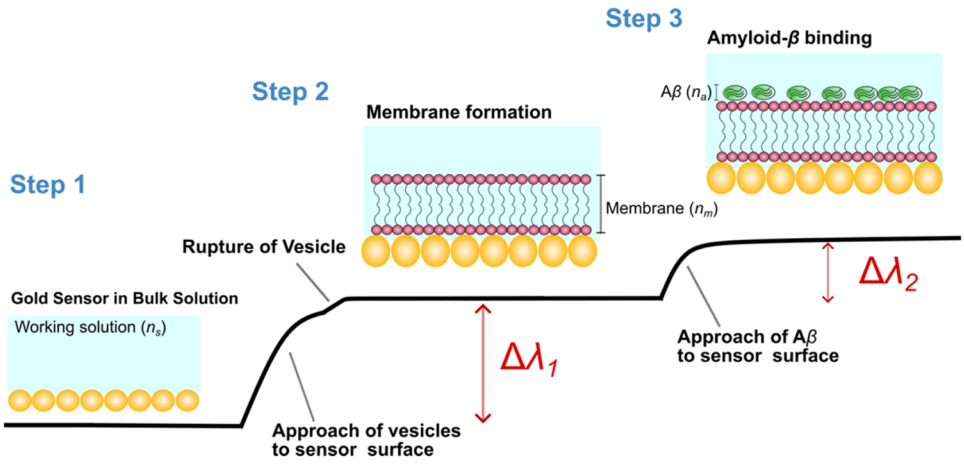

Figure 1. Schematic of the LSPR experiments. From left to right: Step 1. The working solution is continuously flushed over the sensor surface, circulating the LSPR system. Step 2: The injection and rupture of lipid vesicles produce lipid membranes, resulting in an $\Delta\lambda_1$. Step 3: The injection and binding of Aβ to the membrane-covered sensor surface produces $\Delta\lambda_2$.

induces alteration of the dielectric environment, thereby generating the LSPR wavelength shift $\Delta\lambda$, which depends on the refractive index n and thickness of adsorbates d according to eq 1. Therefore, the binding of molecules can be quantified as the thickness of the adsorbate layer.[50] To evaluate the thickness of the membrane and amyloid proteins bound to the LSPR sensor, the m, δ, and refractive index (RI) change Δn require estimation and measurement. The determination of these parameters has been included in the Supporting Information.

Detection of Lipid Membranes and Protein Bindings with LSPR. The LSPR system was perfused with a working solution during an entire experiment process. Before injecting the lipid solutions, 80% isopropanol (IPA)/water (v/v) solution was injected into the system three times to remove bubbles in the system at a pump speed of 150 μL/min. One injection of 80% IPA induced a pulse signal, showing an acute increase in the LSPR wavelength. After three times of 80% IPA injection, the LSPR signal returned to the baseline. As a stable baseline was achieved, the pump speed of the working solution was tuned to 20 μL/min. Then, the system was ready to use for the injection of lipid vesicles and Aβ1−42.

To investigate the effect of trehalose on the membrane properties and Aβ-membrane binding, three working solutions were prepared: (1) 150 mM NaCl 20 mM HEPES, pH 7.4, (2) 50 mM trehalose 150 mM NaCl 20 mM HEPES, pH 7.4, (3) 100 mM trehalose 150 mM NaCl 20 mM HEPES, pH 7.4.

As shown in Figure 1, the working solutions (RI = n_s) acted as a background for the membrane and protein binding signals and were maintained the same for each experiment. The flow speed in the entire experiment was kept at 20 μL/min. Each experiment consisted of two types of injections in sequence: vesicle injection followed by Aβ1−42 injection. First, 200 μL of 0.5 mg/mL lipid vesicles composed of POPC, DPPC, and cholesterol were injected into the system and transferred to the sensor at 20 μL/min. The vesicle injection was repeated 3−4 times to ensure the full coverage of membranes on the sensor surface. The injection of lipid vesicles and membrane formation on the sensor produced a wavelength shift ($\Delta\lambda_1$) as the first LSPR signal. After a 20−30 min wait time for vesicle rupture and membrane stabilization, 200 μL of 50 μM Aβ1−42 was injected and transferred to the membrane-covered sensor at 20 μL/min. The binding of Aβ to the membrane generated the second LSPR wavelength ($\Delta\lambda_2$). As the Aβ injection finished, the experiment was stopped after 20 min.

AFM Imaging. AFM (JPK NanoWizard II, Bruker) was used to image the surface topography of the gold sensor surface and lipid membranes in the hydrated and dehydrated states. The membranes were deposited on LPSR sensors following the protocols for LSPR membranes. The hydrated membranes were imaged in liquid by qp-BioAC AFM probes (NanoSensors) in tapping mode at 25−35 kHz resonance frequency. The nominal spring constant of the probes was 0.3 N/m. The LSPR gold sensor and dehydrated membranes on the sensor surface were imaged in tapping mode in the air by silicon PPP-NCH probes (NanoSensors), with a nominal spring constant of 42 N/m and resonance frequency of 298 kHz. The dehydrated membranes on the LSPR sensors were imaged as soon as the liquid was observed to evaporate. Depending on the humidity in the experimental environment, wait times varied but usually lasted 5−10 min. Surface roughness was calculated with Gwyddion software.

RESULTS AND DISCUSSION

Determination of Membrane Thickness by LSPR. Given that the RI of cholesterol is 1.47[52] and the RI of DPPC is 1.478,[53,54] we assumed that the RI of the lipid membrane composed of POPC, DPPC, and cholesterol was approximately 1.48, within the normal range for biological membranes reported in previous studies.[49] Based on eq 1, the thickness of lipid membranes (d_m) can be calculated by

$$d_m = -\delta \ln\left[1 - \frac{\Delta\lambda_1}{m(n_m - n_s)}\right] \quad (2)$$

where $\Delta\lambda_1$ is the wavelength shift induced by the binding of the lipids.

The estimated membrane thickness in 150 mM NaCl solution (RI = 1.333) is 4.02 ± 0.20 nm (n = 11), as shown in Figure 2. However, the membrane thickness is significantly decreased to 2.53 ± 0.09 nm in 50 mM Trehalose (n = 13) and 2.38 ± 0.13 nm in 100 mM Trehalose solution (n = 14) (Tukey's Test, $p < 0.001$) (Table 1).

These results indicate that the trehalose accumulation at the water/membrane interface decreases membrane thickness. Previous simulation studies have also noted a reduction in

https://doi.org/10.1021/acsomega.4c07038
ACS Omega 2025, 10, 12872−12879

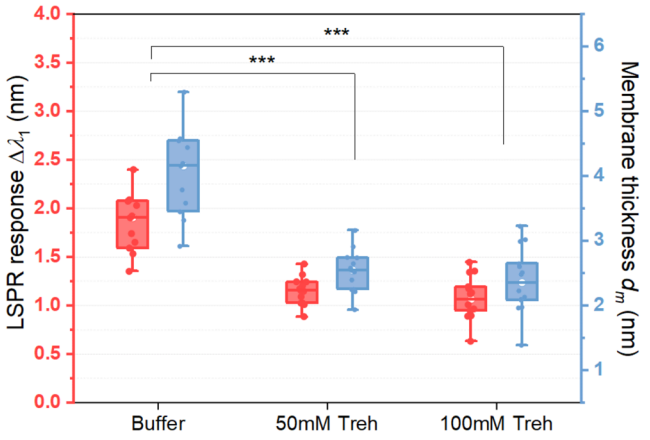

Figure 2. LSPR response to membrane formation ($\Delta\lambda_1$) and corresponding membrane thickness (d_m) measured in working buffers 1, 2, and 3. Red: $\Delta\lambda_1$. Blue: membrane thickness. Treh, trehalose. The corresponding values are shown in Table 1.

Table 1. Lipid-Induced LSPR Response and Membrane Thickness

	NaCl buffer	50 mM Treh-NaCl	100 mM Treh-NaCl
$\Delta\lambda_1$ (nm)	1.84 ± 0.09	1.15 ± 0.04	1.07 ± 0.06
d_m (nm)	4.02 ± 0.20	2.53 ± 0.09	2.38 ± 0.13

membrane thickness induced by trehalose.[41,45,55] It was found that concentrated trehalose, such as 1 M,[41] was necessary in simulations to observe significant changes in lipid membranes,[41,55] as the effect of 100 mM trehalose on membranes was subtle in earlier simulation studies. Whereas simulation results showed that the thickness reduction in the membrane is less than 0.5 nm despite higher concentrations of trehalose,[41,55] it reaches and even exceeds 1.5 nm in 50 and 100 mM trehalose in our experimental studies. The dramatic decrease in membrane thickness in our measurement could be attributed to the improved membrane fluidity due to trehalose's membrane modulation, which has also been reported in previous studies.[56] This highlights the significant impact of trehalose on the mechanical properties of lipid membranes experimentally, even at millimolar levels, in a fully hydrated environment. Additionally, it is worth noting that while 100 mM trehalose is twice the concentration of 50 mM trehalose, both concentrations have similar effects on the membrane. This observation suggests that the thinning of the lipid membrane may reach saturation at a critical concentration of trehalose under hydration conditions.

AFM Imaging Membranes on LSPR Sensors. *Hydrated Membrane.* The gold sensor and membrane-covered sensor surface were imaged by AFM, as shown in Figure 3. The LSPR sensors are mainly composed of spheroid gold nanoparticles with diameters ranging between 80 and 100 nm (Figure 3a), with a surface roughness of 22.14 nm. The rupture of lipid vesicles at the sensor surface produced lipid bilayers. As shown in Figure 3b, the membrane successfully covered gold nanoparticles on the sensor in 150 mM NaCl, leading to a decreased surface roughness of 697.67 pm. In 100 mM Trehalose-NaCl solution, the lipid bilayer also formed and the surface roughness is 1.26 nm (Figure 3c). However, despite that the sensor surfaces were almost fully covered by the lipid membrane with very few vesicle residues left, they still remained uneven due to the presence of grooves, as shown in Figure 3b,3c. These grooves appeared due to the exceptional roughness on the original sensor surface. Overall, the AFM images confirmed that the vesicles reached the gold surface and successfully formed lipid bilayers by rupturing in NaCl and Trehalose-NaCl solutions without the assistance of other agents.

Dehydrated Membranes. To investigate the effect of trehalose on lipid membranes, other than reducing their thickness, the dehydrated membranes were imaged by AFM (Figure 4). Figure 4a shows the self-assembly and crystallization of the NaCl-lipid molecules during dehydration. The degradation of the lipid membrane led to the exposure of the gold nanoparticles of the sensor. However, the lipids maintained their bilayer structure during dehydration in a 100 mM trehalose solution, forming the membrane plateau islands shown in Figure 4b. This suggests that trehalose helps maintain the membrane morphology during dehydration, as

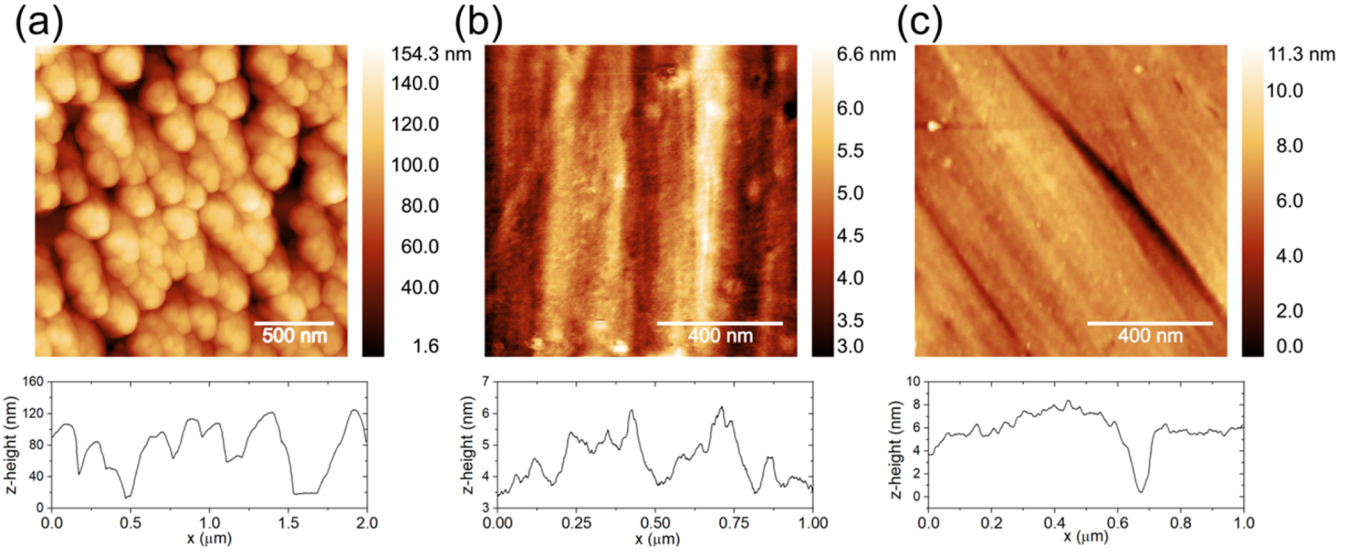

Figure 3. AFM images and cross sections of the LPSR sensor and membranes on the sensors. (a) Bare gold sensor. (b) Lipid membrane formed on the sensor in 150 mM NaCl. (c) Lipid membrane formed on the sensor in 100 mM Trehalose-NaCl solution.

https://doi.org/10.1021/acsomega.4c07038
ACS Omega 2025, 10, 12872−12879

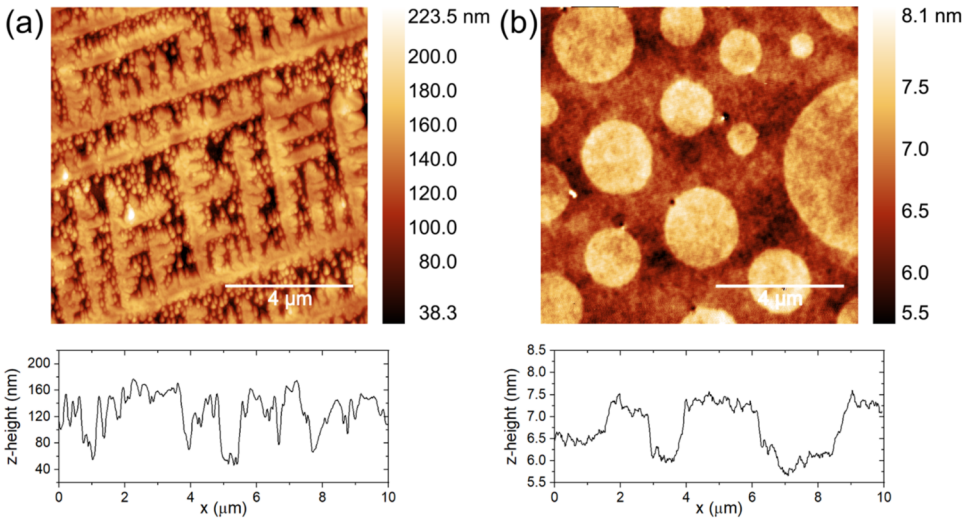

Figure 4. AFM images and cross sections of dehydrated membranes on gold sensors. (a) Dehydrated membrane in 150 mM NaCl solution. (b) Dehydrated membrane in 100 mM Trehalose-NaCl solution. Scale bars: 4 μm.

reported in previous studies.[41] Moreover, the cross section in Figure 4b indicates a membrane height of approximately 1.5 nm. This is lower than the height in the hydrated membrane (2.38 nm) in 100 mM trehalose, as estimated by the LSPR response. It implies that trehalose decreased the membrane thickness, which was further decreased by dehydration. Recent simulations showed that the interaction between trehalose and lipid headgroups depends on the water content level.[41] The water loss enhanced the trehalose-lipid interaction, increasing the distance between lipid molecules and attenuating the fluid-to-gel phase transition induced by dehydration.[41]

Quantitative Estimation of the Aβ Adsorbate Layer by LSPR. After lipid membrane formation on the LSPR sensors, generating the first LSPR signal $\Delta\lambda_1$, the binding of Aβ1−42 peptides induces the second LSPR signal $\Delta\lambda_2$, as indicated in Figure 1. Determining the number of proteins that bind to the membrane from the LSPR response is challenging due to the complex density, geometry, and dimensions of amyloid binding on membranes.[57] However, as shown in Figure 5, the binding

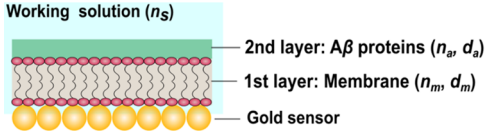

Figure 5. Model for LSPR binding layers.

of the amyloid proteins to the membrane can be simplified as a condensed layer. This is the second adsorbate layer, with thickness d_a on the membrane-covered surface of the LSPR sensor, quantifying bound proteins.[50,57]

The LSPR signal $\Delta\lambda_2$ generated by the binding of the Aβ1−42 protein to the membrane layer of thickness d_m is determined by eq 3[50]

$$\Delta\lambda_2 = m(n_a - n_s)\left[1-\exp\left(-\frac{d_a}{\delta}\right)\right]\exp\left(-\frac{d_m}{\delta}\right) \quad (3)$$

where n_a is the RI of amyloid, which is 1.53 [40]. Based on eq 3, the thickness of the Aβ1−42 layer d_a can be derived as

$$d_a = -\delta \ln\left[1-\frac{\Delta\lambda_2 \exp\left(\frac{d_m}{\delta}\right)}{m(n_a - n_s)}\right] \quad (4)$$

It can be rewritten into eq 5 according to eq 1

$$d_a = -\delta \ln\left[1-\frac{\Delta\lambda_2\left(1-\frac{\Delta\lambda_1}{m(n_m - n_s)}\right)^{-1}}{m(n_a - n_s)}\right] \quad (5)$$

Either eq 4 or eq 5 can be used to calculate the thickness of the second layer of Aβ1−42. The thickness parameter d_a is used to estimate the quantity of proteins bound to the lipid membrane.

As shown in Figure 6, the Aβ-induced LSPR response $\Delta\lambda_2$ decreased in the trehalose solutions. It decreased from 0.39 ± 0.03 nm (mean ± SEM) in the NaCl control buffer to 0.33 ± 0.03 nm in 50 mM and 0.29 ± 0.02 nm in 100 mM trehalose-NaCl solutions (Tukey test, $p < 0.05$); this dose-dependent behavior is shown in Table 2.

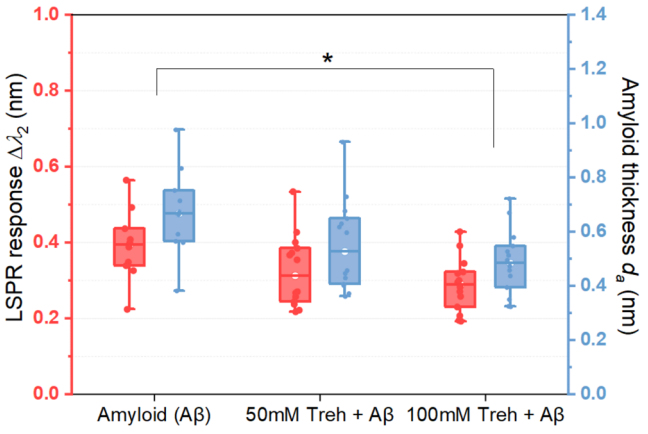

Figure 6. LSPR response to amyloid binding to lipid membranes $\Delta\lambda_2$ and corresponding layer thickness d_a in working buffers 1, 2, and 3. Red: $\Delta\lambda_2$. Blue: Amyloid layer thickness d_a. The corresponding values are given in Table 2.

https://doi.org/10.1021/acsomega.4c07038
ACS Omega 2025, 10, 12872−12879

Table 2. Aβ-Induced LSPR Response and Layer Thickness

	Aβ	50 mM Treh + Aβ	100 mM Treh + Aβ
$\Delta\lambda_2$ (nm)	0.39 ± 0.03	0.33 ± 0.03	0.29 ± 0.02
d_a (nm)	0.67 ± 0.05	0.55 ± 0.04	0.49 ± 0.03

eq 5 was used to compute d_a according to the LSPR signals collected in the solution with and without trehalose and found the decline of Aβ thickness d_a in trehalose solutions, aligned with the trend of $\Delta\lambda_2$. Remarkably, d_a (0.67 ± 0.05 nm, n = 10) in NaCl was significantly decreased to 0.49 ± 0.03 nm (n = 14) in 100 mM Trehalose (Tukey's test, $p < 0.05$), suggesting fewer Aβ1−42 peptides bound to the lipid membrane in 100 mM trehalose. This implies that 100 mM trehalose effectively reduced the binding of Aβ to the lipid membrane. Our result is consistent with a study by Izmitli et al. in which simulation studies reported that fewer Aβ1−40 peptides were inserted into anionic DPPG monolayers in a trehalose solution than in water; this was attributed to the energy profile at the subphase-lipid interface.[46] The smaller difference in free energy at the water−lipid interface compared to the trehalose-lipid interface makes the peptide insertion more energetically favorable, leading to more insertions in water over trehalose. In addition, the accumulation and interaction of trehalose with lipid headgroups may increase the viscosity near the lipid membranes. This is driven by the trehalose concentration and increases the resistance of peptides to access the membrane, thereby inhibiting the adsorption of Aβ to lipid membranes.

Previous studies found that Aβ peptides penetrated deeper into lipids in water than in trehalose, leading to severe membrane expansion.[46] Our recent study demonstrated that the Aβ-induced membrane damage was reduced by trehalose,[28] which indicates that trehalose can enhance membrane stability as Aβ insertion occurs. These results and our current findings suggest that the protective role of trehalose is attributed not only to its interference with peptides but also to its modulation of membrane properties, protecting the biomembranes from Aβ neurotoxicity by reducing the amyloid-membrane binding. Transgenic mouse studies by Portbury et al. reported the improvement in mice's cognition after daily 2% trehalose intake for a month, while the mechanisms were not fully understood.[58] Our studies may help understand the protective role of trehalose against amyloid toxicity in neuronal systems from a perspective of membrane protection.

In this work, we used a simple three-component lipid model to test the protective effect of trehalose against the nonspecific binding of amyloid to the membrane. In the future, more complex biologically relevant lipid systems should be explored in this context. A vast amount of data is currently available on amyloid interactions with biomembranes.[8−17,59−65] This work has included the study of the role of membranes in amyloid aggregation and toxicity:[60,61] indicating the role of lipid composition, especially the inclusion of gangliosides and sphingomyelin;[62,63,66] the presence of cholesterol;[59,66] nanoscale lipid rafts, and many other parameters that affect amyloid-membrane binding;[8−17,64,65] however, these studies do not explore membrane-protective molecules. The contribution of our study is that we demonstrate that the membranes can be protected from amyloid toxicity with trehalose, even in simple lipid models, by reducing the level of binding of amyloid to the membrane.

CONCLUSIONS

The influence of trehalose on model lipid membranes (DPPC-POPC-Chol) and its effect on the binding of Aβ1−42 to a lipid membrane was studied. The LSPR results showed that trehalose can effectively reduce nonspecific binding of Aβ1−42 to the membranes in a concentration-dependent manner, which supports our previous report that trehalose reduces the membrane damage induced by Aβ1−42 in electrophysiology experiments.[28] The trehalose effect could potentially attenuate Aβ-related membrane destruction and cytotoxicity in biomembranes, and this knowledge can be beneficial for the development of future membrane-targeted preventive strategies for Alzheimer's Disease. This work significantly fills the void of experimental studies in trehalose-related Aβ-membrane studies and explores the quantitative analysis for the nonspecific binding of biomolecules in LSPR-dominated biosensing.

ASSOCIATED CONTENT

Supporting Information

The Supporting Information is available free of charge at https://pubs.acs.org/doi/10.1021/acsomega.4c07038.

Methods and materials to determine the parameters of LSPR sensors (PDF)

AUTHOR INFORMATION

Corresponding Author

Zoya Leonenko − *Department of Physics & Astronomy, University of Waterloo, Waterloo, Ontario N2L 3G1, Canada; Department of Biology, University of Waterloo, Waterloo, Ontario N2L 3G1, Canada; Waterloo Institute for Nanotechnology, Waterloo, Ontario N2L 3G1, Canada*; Email: zleonenk@uwaterloo.ca

Authors

Yue Xu − *Department of Physics & Astronomy, University of Waterloo, Waterloo, Ontario N2L 3G1, Canada*; orcid.org/0009-0001-7874-7994

Danielle M. McRae − *Department of Physics & Astronomy, University of Waterloo, Waterloo, Ontario N2L 3G1, Canada*

Complete contact information is available at: https://pubs.acs.org/10.1021/acsomega.4c07038

Notes

The authors declare no competing financial interest.

ACKNOWLEDGMENTS

The authors appreciate the funding from the Natural Sciences and Engineering Research Council of Canada (NSERC) for this study.

REFERENCES

(1) Richards, A. B.; Krakowka, S.; Dexter, L. B.; Schmid, H.; Wolterbeek, A. P. M.; Waalkens-Berendsen, D. H.; Shigoyuki, A.; Kurimoto, M. Trehalose: a review of properties, history of use and human tolerance, and results of multiple safety studies. *Food Chem. Toxicol.* **2002**, *40* (7), 871−898.

(2) Khalifeh, M.; Barreto, G. E.; Sahebkar, A. Therapeutic potential of trehalose in neurodegenerative diseases: the knowns and unknowns. *Neural Regener. Res.* **2021**, *16* (10), 2026−2027.

(3) Pupyshev, A. B.; Klyushnik, T. P.; Akopyan, A. A.; Singh, S. K.; Tikhonova, M. A. Disaccharide trehalose in experimental therapies for neurodegenerative disorders: Molecular targets and translational potential. *Pharmacol. Res.* **2022**, *183*, No. 106373.
(4) Rushworth, J. V.; Hooper, N. M. Lipid Rafts: Linking Alzheimer's Amyloid-β Production, Aggregation, and Toxicity at Neuronal Membranes. *Int. J. Alzheimer's Dis.* **2010**, *2011*, No. 603052.
(5) Cecchi, C.; Stefani, M. The amyloid-cell membrane system. The interplay between the biophysical features of oligomers/fibrils and cell membrane defines amyloid toxicity. *Biophys. Chem.* **2013**, *182*, 30−43.
(6) Hardy, J. A.; Higgins, G. A. Alzheimer's Disease: The Amyloid Cascade Hypothesis. *Science* **1992**, *256* (5054), 184−185.
(7) Fessler, M. B.; Parks, J. S. Intracellular lipid flux and membrane microdomains as organizing principles in inflammatory cell signaling. *J. Immunol.* **2011**, *187* (4), 1529−1535.
(8) Eckert, G. P.; Wood, W. G.; Muller, W. E. Lipid Membranes and beta-Amyloid: A Harmful Connection. *Curr. Protein Peptide Sci.* **2010**, *11* (5), 319−325.
(9) Kim, S.-I.; Yi, J.-S.; Ko, Y.-G. Amyloid β oligomerization is induced by brain lipid rafts. *J. Cell. Biochem.* **2006**, *99* (3), 878−889.
(10) Hertel, C.; Terzi, E.; Hauser, N.; Jakob-Røtne, R.; Seelig, J.; Kemp, J. A. Inhibition of the electrostatic interaction between β-amyloid peptide and membranes prevents β-amyloid-induced toxicity. *Proc. Natl. Acad. Sci. U.S.A.* **1997**, *94* (17), 9412−9416.
(11) Drolle, E.; Negoda, A.; Hammond, K.; Pavlov, E.; Leonenko, Z. Changes in lipid membranes may trigger amyloid toxicity in Alzheimer's disease. *PLoS One* **2017**, *12* (8), No. e0182194.
(12) Drolle, E.; Hane, F.; Lee, B.; Leonenko, Z. Atomic force microscopy to study molecular mechanisms of amyloid fibril formation and toxicity in Alzheimer's disease. *Drug Metab. Rev.* **2014**, *46* (2), 207−223.
(13) Siniscalco, D.; Francius, G.; Tarek, M.; Bali, S. K.; Laprévote, O.; Malaplate, C.; Oster, T.; Pauron, L.; Quilès, F. Molecular Insights for Alzheimer's Disease: An Unexplored Storyline on the Nanoscale Impact of Nascent Aβ1−42 toward the Lipid Membrane. *ACS Appl. Mater. Interfaces* **2023**, *15* (14), 17507−17517.
(14) Mrdenovic, D.; Pieta, I. S.; Nowakowski, R.; Kutner, W.; Lipkowski, J.; Pieta, P. Amyloid β interaction with model cell membranes − What are the toxicity-defining properties of amyloid β? *Int. J. Biol. Macromol.* **2022**, *200*, 520−531.
(15) Mrdenovic, D.; Zarzycki, P.; Majewska, M.; Pieta, I. S.; Nowakowski, R.; Kutner, W.; Lipkowski, J.; Pieta, P. Inhibition of Amyloid β-Induced Lipid Membrane Permeation and Amyloid β Aggregation by K162. *ACS Chem. Neurosci.* **2021**, *12* (3), 531−541.
(16) Errico, S.; Lucchesi, G.; Odino, D.; Muscat, S.; Capitini, C.; Bugelli, C.; Canale, C.; Ferrando, R.; Grasso, G.; Barbut, D.; et al. Making biological membrane resistant to the toxicity of misfolded protein oligomers: a lesson from trodusquemine. *Nanoscale* **2020**, *12* (44), 22596−22614.
(17) Mrdenovic, D.; Majewska, M.; Pieta, I. S.; Bernatowicz, P.; Nowakowski, R.; Kutner, W.; Lipkowski, J.; Pieta, P. Size-Dependent Interaction of Amyloid β Oligomers with Brain Total Lipid Extract Bilayer—Fibrillation Versus Membrane Destruction. *Langmuir* **2019**, *35* (36), 11940−11949.
(18) Breijyeh, Z.; Karaman, R. Comprehensive Review on Alzheimer's Disease: Causes and Treatment. *Molecules* **2020**, *25* (24), No. 5789.
(19) Doody, R. S.; Raman, R.; Farlow, M.; Iwatsubo, T.; Vellas, B.; Joffe, S.; Kieburtz, K.; He, F.; Sun, X.; Thomas, R. G.; et al. A Phase 3 Trial of Semagacestat for Treatment of Alzheimer's Disease. *N. Engl. J. Med.* **2013**, *369* (4), 341−350.
(20) Reddy, A. S.; Izmitli, A.; de Pablo, J. J. Effect of trehalose on amyloid β (29−40)-membrane interaction. *J. Chem. Phys.* **2009**, *131* (8), No. 085101.
(21) Torres, M.; Price, S. L.; Fiol-deRoque, M. A.; Marcilla-Etxenike, A.; Ahyayauch, H.; Barceló-Coblijn, G.; Terés, S.; Katsouri, L.; Ordinas, M.; López, D. J.; et al. Membrane lipid modifications and therapeutic effects mediated by hydroxydocosahexaenoic acid on Alzheimer's disease. *Biochim. Biophys. Acta, Biomembr.* **2014**, *1838* (6), 1680−1692.
(22) Dies, H.; Toppozini, L.; Rheinstädter, M. C. The Interaction between Amyloid-β Peptides and Anionic Lipid Membranes Containing Cholesterol and Melatonin. *PLoS One* **2014**, *9* (6), No. e99124.
(23) Drolle, E.; Kučerka, N.; Hoopes, M. I.; Choi, Y.; Katsaras, J.; Karttunen, M.; Leonenko, Z. Effect of melatonin and cholesterol on the structure of DOPC and DPPC membranes. *Biochim. Biophys. Acta, Biomembr.* **2013**, *1828* (9), 2247−2254.
(24) Khalifeh, M.; Barreto, G. E.; Sahebkar, A. Trehalose as a promising therapeutic candidate for the treatment of Parkinson's disease. *Br. J. Pharmacol.* **2019**, *176* (9), 1173−1189.
(25) Liu, R.; Barkhordarian, H.; Emadi, S.; Park, C. B.; Sierks, M. R. Trehalose differentially inhibits aggregation and neurotoxicity of beta-amyloid 40 and 42. *Neurobiol. Dis.* **2005**, *20* (1), 74−81.
(26) Liu, F.-F.; Ji, L.; Dong, X.-Y.; Sun, Y. Molecular Insight into the Inhibition Effect of Trehalose on the Nucleation and Elongation of Amyloid β-Peptide Oligomers. *J. Phys. Chem. B* **2009**, *113* (32), 11320−11329.
(27) Khan, S. H.; Kumar, R. Trehalose induced conformational changes in the amyloid-β peptide. *Pathol. Res. Practice* **2017**, *213* (6), 643−648.
(28) Xu, Y.; Filice, C. T.; Leonenko, Z. Protective effect of trehalose sugar on amyloid-membrane interactions using BLM electrophysiology. *Biophys. J.* **2024**, *123* (12), 1690−1704.
(29) Tian, Y.; Liang, R.; Kumar, A.; Szwedziak, P.; Viles, J. H. 3D-visualization of amyloid-β oligomer interactions with lipid membranes by cryo-electron tomography. *Chem. Sci.* **2021**, *12* (20), 6896−6907.
(30) Bhatia, R.; Lin, H.; Lal, R. Fresh and globular amyloid beta protein (1−42) induces rapid cellular degeneration: evidence for AbetaP channel-mediated cellular toxicity. *FASEB J.* **2000**, *14* (9), 1233−1243.
(31) Morkuniene, R.; Cizas, P.; Jankeviciute, S.; Petrolis, R.; Arandarcikaite, O.; Krisciukaitis, A.; Borutaite, V. Small Aβ1−42 oligomer-induced membrane depolarization of neuronal and microglial cells: Role of N-methyl-D-aspartate receptors. *J. Neurosci. Res.* **2015**, *93* (3), 475−486.
(32) Klein, A. M.; Kowall, N. W.; Ferrante, R. J. Neurotoxicity and oxidative damage of beta amyloid 1−42 versus beta amyloid 1−40 in the mouse cerebral cortex. *Ann. N. Y. Acad. Sci.* **1999**, *893*, 314−320.
(33) Bode, D. C.; Freeley, M.; Nield, J.; Palma, M.; Viles, J. H. Amyloid-β oligomers have a profound detergent-like effect on lipid membrane bilayers, imaged by atomic force and electron microscopy. *J. Biol. Chem.* **2019**, *294* (19), 7566−7572.
(34) Bode, D. C.; Baker, M. D.; Viles, J. H. Ion Channel Formation by Amyloid-β42 Oligomers but Not Amyloid-β40 in Cellular Membranes. *J. Biol. Chem.* **2017**, *292* (4), 1404−1413.
(35) Pereira, C. S.; Lins, R. D.; Chandrasekhar, I.; Freitas, L. C. G.; Hünenberger, P. H. Interaction of the Disaccharide Trehalose with a Phospholipid Bilayer: A Molecular Dynamics Study. *Biophys. J.* **2004**, *86* (4), 2273−2285.
(36) Villarreal, M. A.; Díaz, S. B.; Disalvo, E. A.; Montich, G. G. Molecular dynamics simulation study of the interaction of trehalose with lipid membranes. *Langmuir* **2004**, *20* (18), 7844−7851.
(37) Skibinsky, A.; Venable, R. M.; Pastor, R. W. A molecular dynamics study of the response of lipid bilayers and monolayers to trehalose. *Biophys. J.* **2005**, *89* (6), 4111−4121.
(38) Horta, B. A.; Peric-Hassler, L.; Hunenberger, P. H. Interaction of the disaccharides trehalose and gentiobiose with lipid bilayers: a comparative molecular dynamics study. *J. Mol. Graphics Model.* **2010**, *29* (3), 331−346.
(39) Green, J. L.; Angell, C. A. Phase relations and vitrification in saccharide-water solutions and the trehalose anomaly. *J. Phys. Chem.* **1989**, *93* (8), 2880−2882.
(40) Koster, K. L.; Webb, M. S.; Bryant, G.; Lynch, D. V. Interactions between soluble sugars and POPC (1-palmitoyl-2-oleoylphosphatidylcholine) during dehydration: vitrification of sugars

https://doi.org/10.1021/acsomega.4c07038
ACS Omega 2025, 10, 12872−12879

alters the phase behavior of the phospholipid. *Biochim. Biophys. Acta, Biomembr.* **1994**, *1193* (1), 143−150.
(41) Maiti, A.; Daschakraborty, S. Unraveling the Molecular Mechanisms of Trehalose-Mediated Protection and Stabilization of *Escherichia coli* Lipid Membrane during Desiccation. *J. Phys. Chem. B* **2023**, *127* (20), 4496−4507.
(42) Dahlgren, K. N.; Manelli, A. M.; Stine, W. B.; Baker, L. K.; Krafft, G. A.; LaDu, M. J. Oligomeric and Fibrillar Species of Amyloid-β Peptides Differentially Affect Neuronal Viability*. *J. Biol. Chem.* **2002**, *277* (35), 32046−32053.
(43) Clegg, J. S.; Seitz, P.; Seitz, W.; Hazlewood, C. F. Cellular responses to extreme water loss: The water-replacement hypothesis. *Cryobiology* **1982**, *19* (3), 306−316.
(44) Wolfe, J.; Bryant, G. Freezing, drying, and/or vitrification of membrane- solute-water systems. *Cryobiology* **1999**, *39* (2), 103−129.
(45) Liu, J.; Chen, C.; Lu, C.; Li, W. Different mechanisms on the stabilization of POPC membrane by trehalose upon varied mechanical stress. *J. Mol. Liq.* **2019**, *275*, 839−848.
(46) Izmitli, A.; Schebor, C.; McGovern, M. P.; Reddy, A. S.; Abbott, N. L.; de Pablo, J. J. Effect of trehalose on the interaction of Alzheimer's Abeta-peptide and anionic lipid monolayers. *Biochim. Biophys. Acta, Biomembr.* **2011**, *1808* (1), 26−33.
(47) Willets, K. A.; Duyne, R. P. V. Localized Surface Plasmon Resonance Spectroscopy and Sensing. *Annu. Rev. Phys. Chem.* **2007**, *58* (1), 267−297.
(48) Rupert, D. L. M.; Shelke, G. V.; Emilsson, G.; Claudio, V.; Block, S.; Lässer, C.; Dahlin, A.; Lötvall, J. O.; Bally, M.; Zhdanov, V. P.; Höök, F. Dual-Wavelength Surface Plasmon Resonance for Determining the Size and Concentration of Sub-Populations of Extracellular Vesicles. *Anal. Chem.* **2016**, *88* (20), 9980−9988.
(49) Parkkila, P.; Elderdfi, M.; Bunker, A.; Viitala, T. Biophysical Characterization of Supported Lipid Bilayers Using Parallel Dual-Wavelength Surface Plasmon Resonance and Quartz Crystal Microbalance Measurements. *Langmuir* **2018**, *34* (27), 8081−8091.
(50) Jung, L. S.; Campbell, C. T.; Chinowsky, T. M.; Mar, M. N.; Yee, S. S. Quantitative Interpretation of the Response of Surface Plasmon Resonance Sensors to Adsorbed Films. *Langmuir* **1998**, *14* (19), 5636−5648.
(51) Zhdanov, V. P. Basics of the LSPR Sensors for Soft Matter at Interfaces. *Plasmonics* **2023**, *18* (3), 971−982.
(52) Lafont, S.; Rapaport, H.; Somjen, G. J.; Renault, A.; Howes, P. B.; Kjaer, K.; Als-Nielsen, J.; Leiserowitz, L.; Lahav, M. Monitoring the nucleation of crystalline films of cholesterol on water and in the presence of phospholipid. *J. Phys. Chem. B* **1998**, *102* (5), 761−765.
(53) Kienle, D. F.; de Souza, J. V.; Watkins, E. B.; Kuhl, T. L. Thickness and refractive index of DPPC and DPPE monolayers by multiple-beam interferometry. *Anal. Bioanal. Chem.* **2014**, *406* (19), 4725−4733.
(54) Pusterla, J. M.; Malfatti-Gasperini, A. A.; Puentes-Martinez, X. E.; Cavalcanti, L. P.; Oliveira, R. G. Refractive index and thickness determination in Langmuir monolayers of myelin lipids. *Biochim. Biophys. Acta, Biomembr.* **2017**, *1859* (5), 924−930.
(55) Kumar, A.; Cincotti, A.; Aparicio, S. Insights into the interaction between lipid bilayers and trehalose aqueous solutions. *J. Mol. Liq.* **2020**, *314*, No. 113639.
(56) Aboagla, E. M.-E.; Terada, T. Trehalose-Enhanced Fluidity of the Goat Sperm Membrane and Its Protection During Freezing. *Biol. Reprod.* **2003**, *69* (4), 1245−1250.
(57) Vörös, J. The density and refractive index of adsorbing protein layers. *Biophys. J.* **2004**, *87* (1), 553−561.
(58) Portbury, S. D.; Hare, D. J.; Sgambelloni, C.; Perronnes, K.; Portbury, A. J.; Finkelstein, D. I.; Adlard, P. A. Trehalose Improves Cognition in the Transgenic Tg2576 Mouse Model of Alzheimer's Disease. *J. Alzheimer's Dis.* **2017**, *60* (2), 549−560.
(59) Drolle, E.; Gaikwad, R. M.; Leonenko, Z. Nanoscale electrostatic domains in cholesterol-laden lipid membranes create a target for amyloid binding. *Biophys. J.* **2012**, *103* (4), L27−29.
(60) Rangachari, V.; Dean, D. N.; Rana, P.; Vaidya, A.; Ghosh, P. Cause and consequence of Aβ - Lipid interactions in Alzheimer disease pathogenesis. *Biochim. Biophys. Acta, Biomembr.* **2018**, *1860* (9), 1652−1662.
(61) Sciacca, M. F.; Kotler, S. A.; Brender, J. R.; Chen, J.; Lee, D. K.; Ramamoorthy, A. Two-step mechanism of membrane disruption by Aβ through membrane fragmentation and pore formation. *Biophys. J.* **2012**, *103* (4), 702−710.
(62) Rudajev, V.; Novotny, J. The Role of Lipid Environment in Ganglioside GM1-Induced Amyloid β Aggregation. *Membranes* **2020**, *10* (9), No. 226.
(63) Matsubara, T.; Yasumori, H.; Ito, K.; Shimoaka, T.; Hasegawa, T.; Sato, T. Amyloid-β fibrils assembled on ganglioside-enriched membranes contain both parallel β-sheets and turns. *J. Biol. Chem.* **2018**, *293* (36), 14146−14154.
(64) Kumar, A.; Bullard, R. L.; Patel, P.; Paslay, L. C.; Singh, D.; Bienkiewicz, E. A.; Morgan, S. E.; Rangachari, V. Non-Esterified Fatty Acids Generate Distinct Low-Molecular Weight Amyloid-β (Aβ42) Oligomers along Pathway Different from Fibril Formation. *PLoS One* **2011**, *6* (4), No. e18759.
(65) Sugiura, Y.; Ikeda, K.; Nakano, M. High Membrane Curvature Enhances Binding, Conformational Changes, and Fibrillation of Amyloid-β on Lipid Bilayer Surfaces. *Langmuir* **2015**, *31* (42), 11549−11557.
(66) Kakio, A.; Nishimoto, S.-I.; Yanagisawa, K.; Kozutsumi, Y.; Matsuzaki, K. Cholesterol-dependent Formation of GM1 Ganglioside-bound Amyloid β-Protein, an Endogenous Seed for Alzheimer Amyloid*. *J. Biol. Chem.* **2001**, *276* (27), 24985−24990.

https://doi.org/10.1021/acsomega.4c07038
ACS Omega 2025, 10, 12872−12879